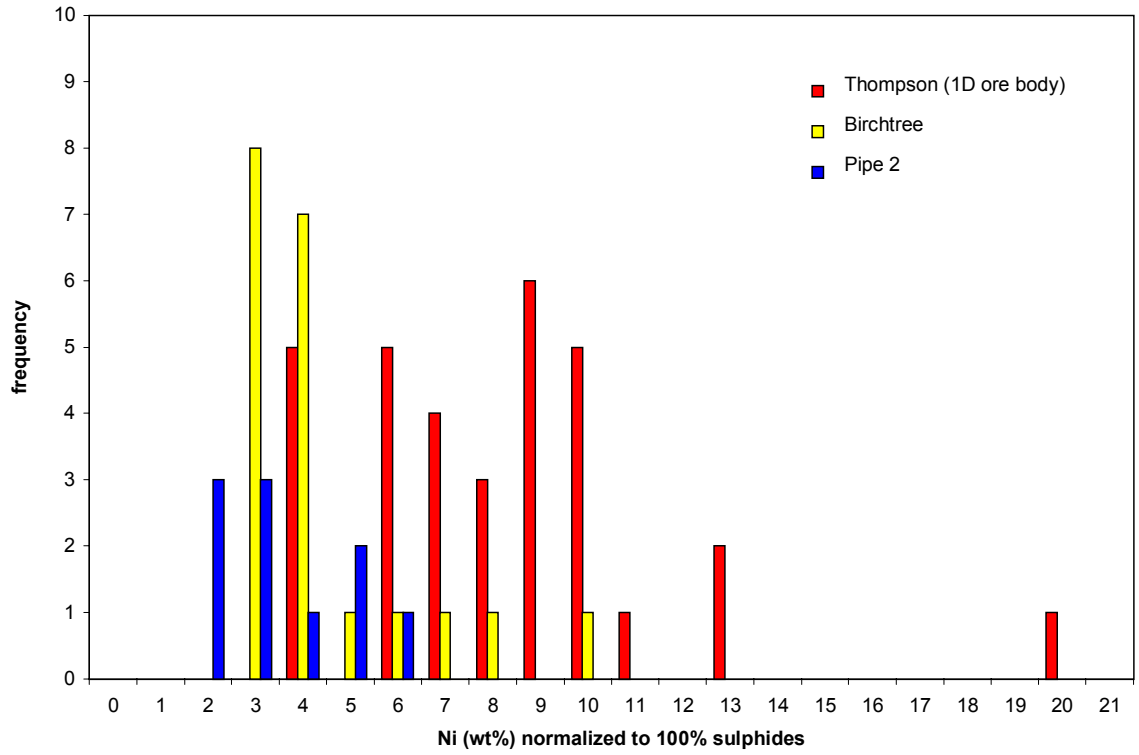

Figure 9.31 Ni concentration of massive and semi-massive sulfides from the TNB, normalized to 100% sulfides. Sulfide classes represented: MS-UB, MS-SED, SMS-SED. From Liwanag (2001).

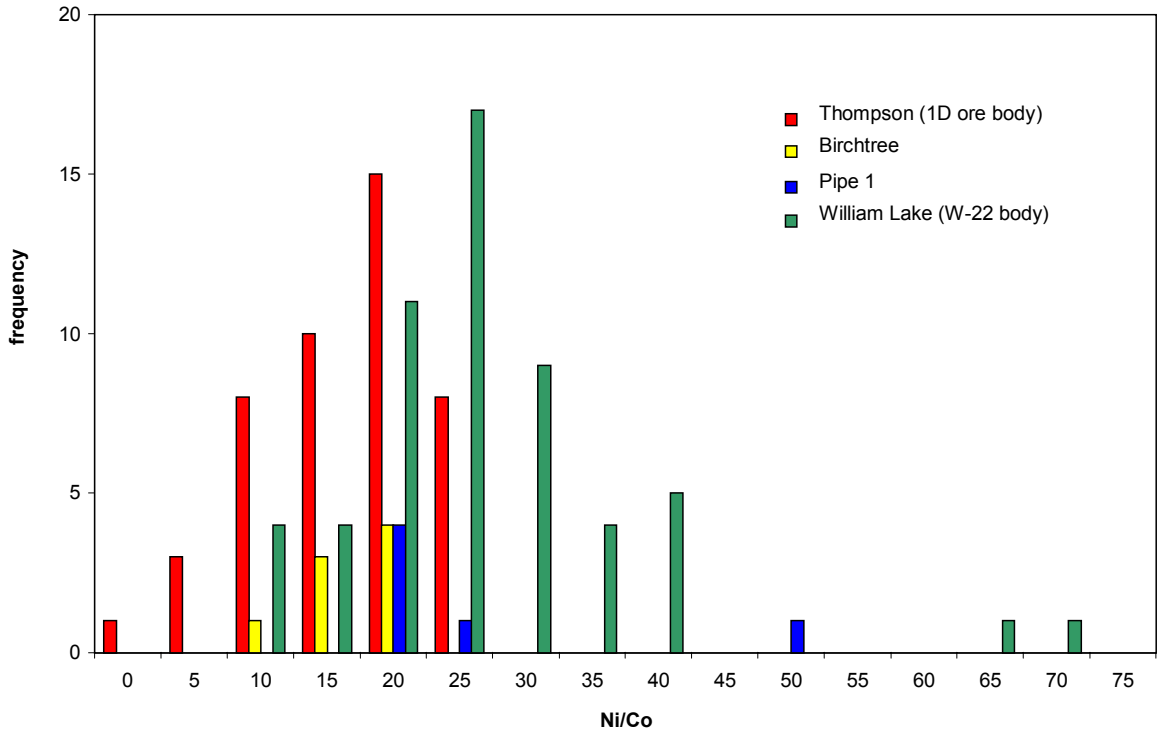

Figure 9.32 Ni/Co ratios of ultramafic bodies from the TNB with the following geochemical parameters: MgO > 24%, S < 5000 ppm, and Se/S x 10^6 < 1000. From Liwanag (2001).

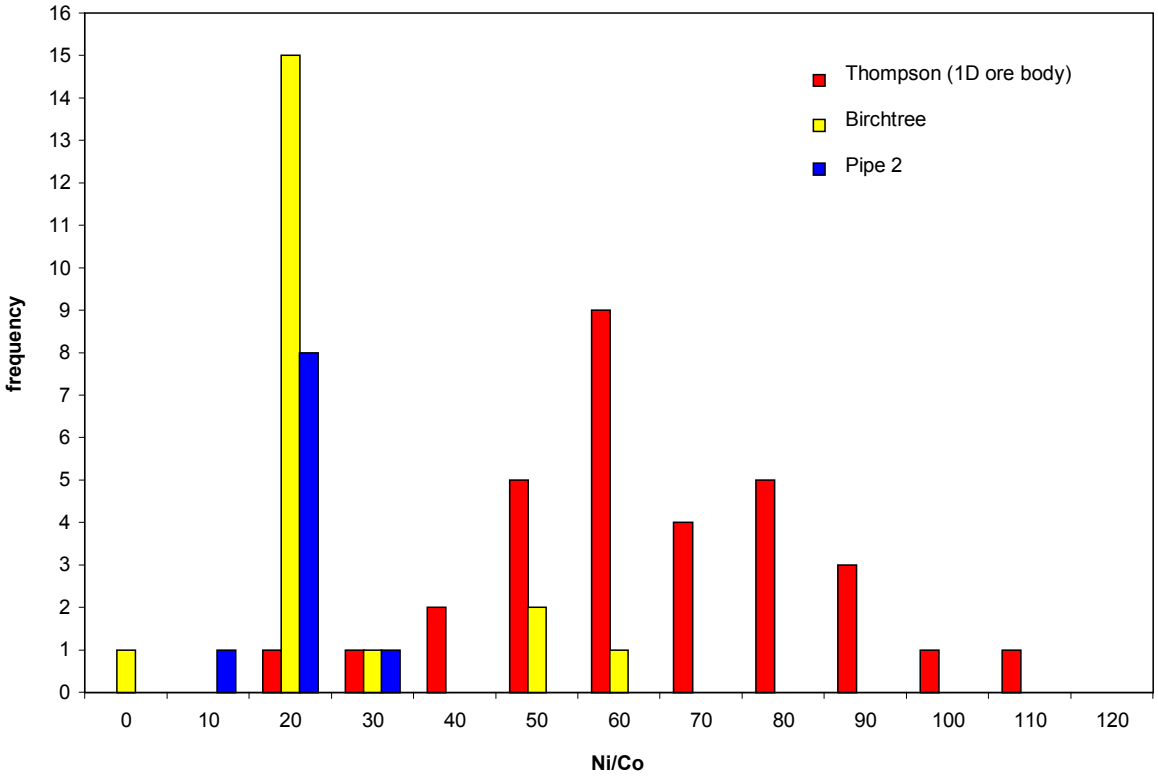

Figure 9.33 Ni/Co ratios of massive and semi-massive sulfides from the TNB. Sulfide classes represented: MS-UB, MS-SED, SMS-SED. From Liwanag (2001).

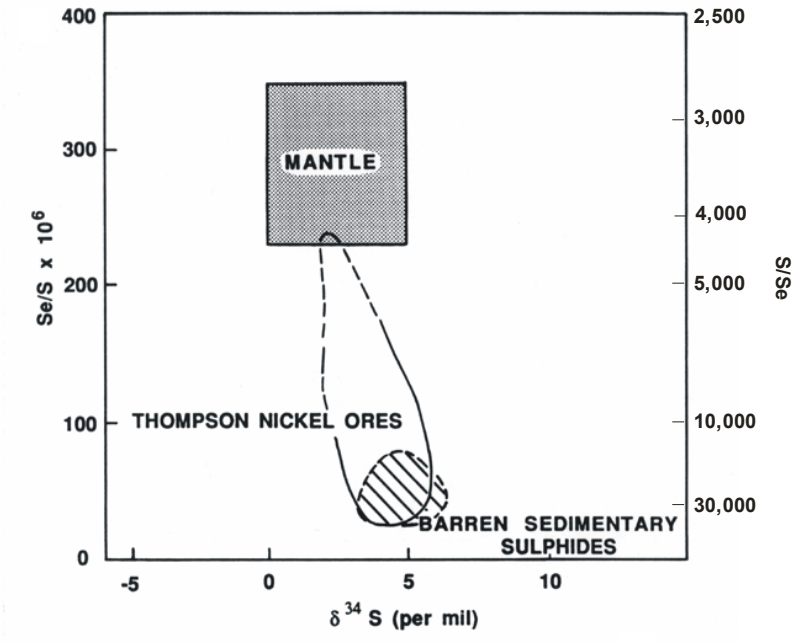

Figure 9.34 Se/S and $\delta^{34}S$ data for Ni sulfide ores and barren sedimentary sulfides from the TNB. From Eckstrand et al. (1989).

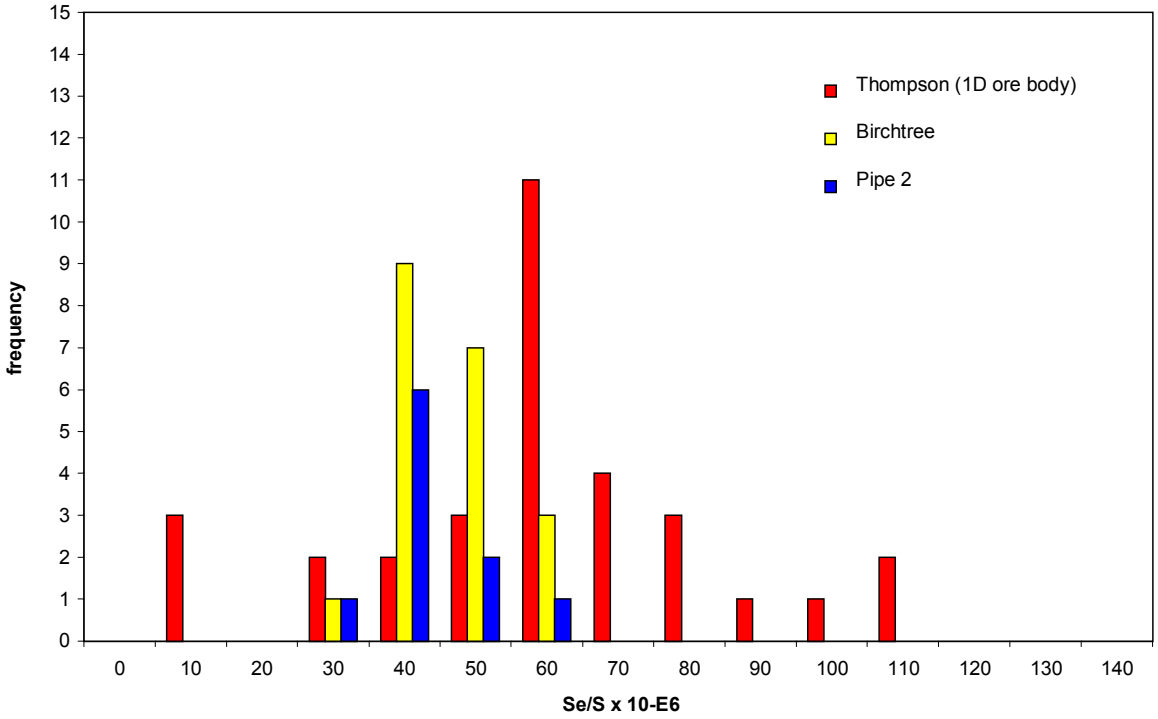

Figure 9.35 Se/S ratios of massive and semi-massive sulfide samples from the TNB. From Liwanag (2001).

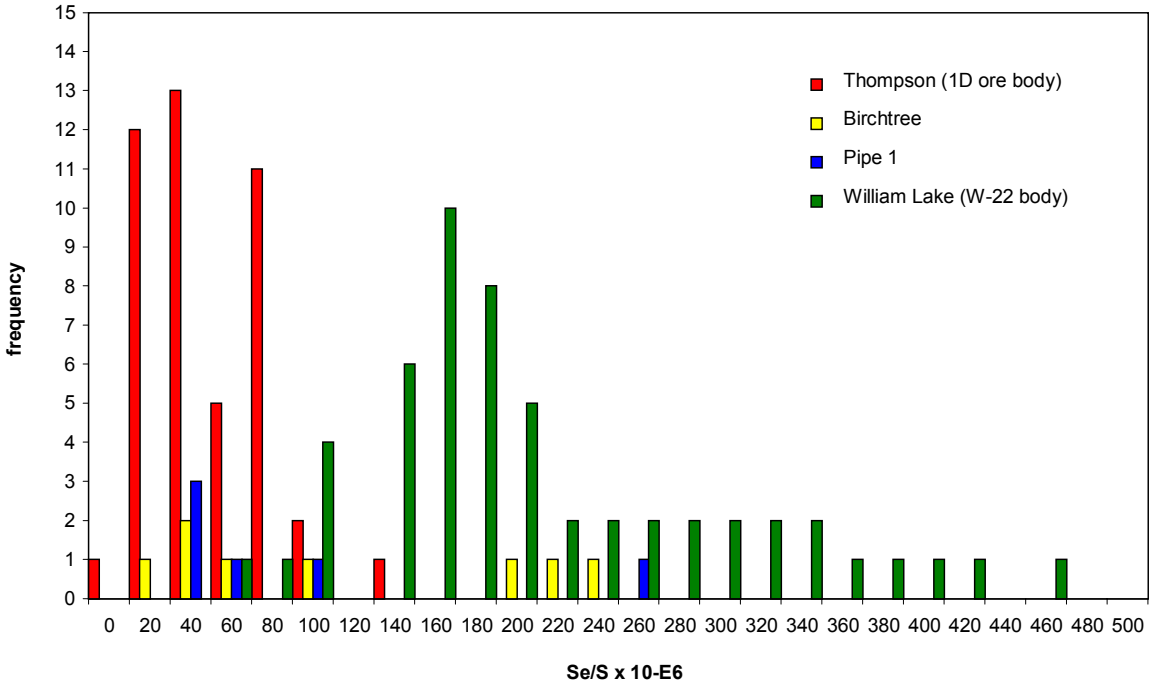

Figure 9.36 Se/S of ultramafic bodies from the TNB with the following geochemical parameters: MgO > 24%, S < 5000 ppm, and Se/S x 10^6 < 1000. From Liwanag (2001).

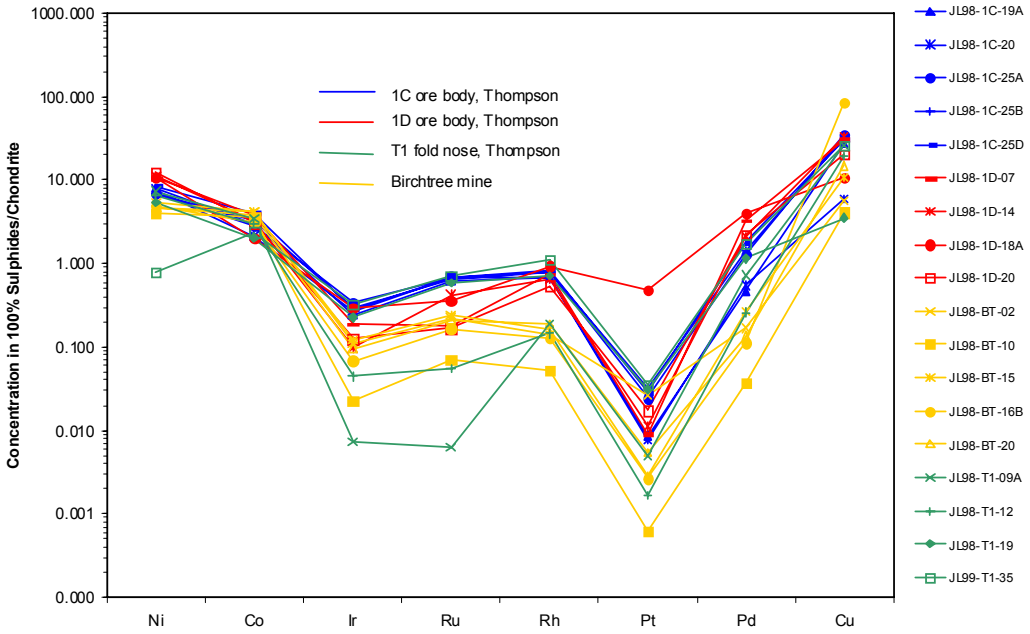

Figure 9.37 Chondrite-normalized plot of chalcophile element concentrations in massive and semi-massive sulfide samples from the TNB (this study). Data are recalculated to 100% sulfide and then normalized by the chondritic abundances for each element. From Liwanag (2001).

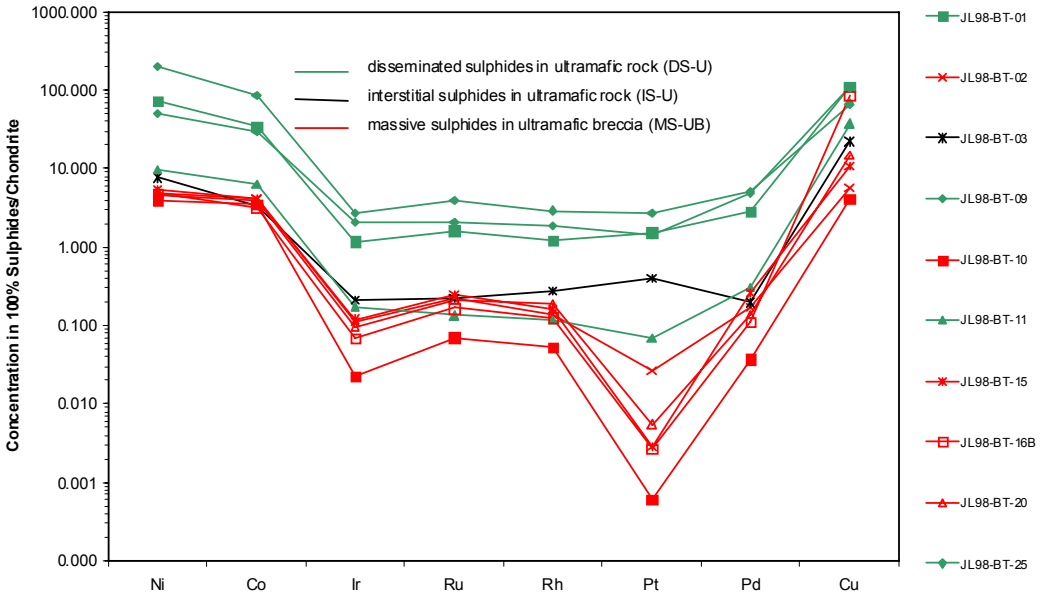

Figure 9.38 Chondrite-normalized plot of chalcophile element concentrations in samples from Birchtree Mine (this study). From Liwanag (2001).

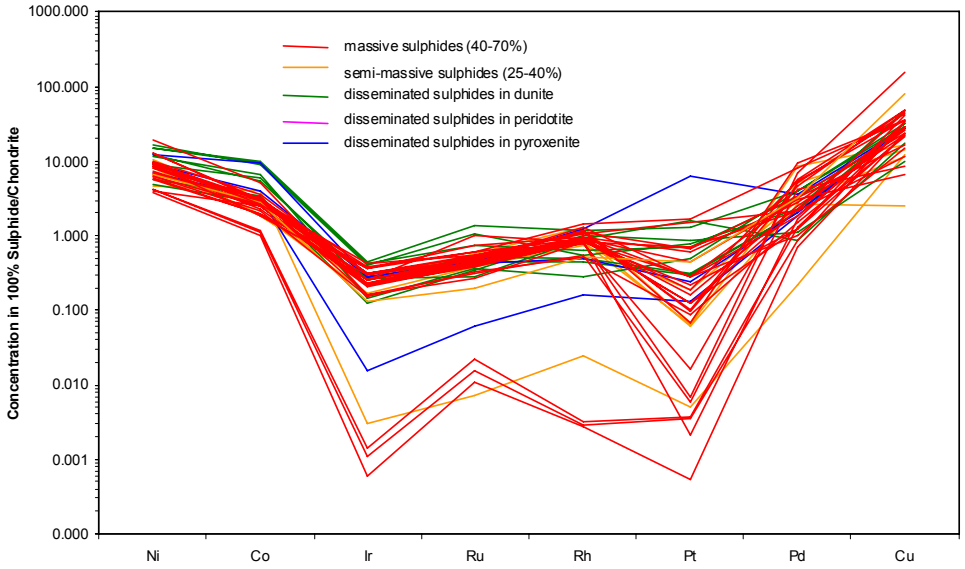

Figure 9.39 Chondrite-normalized plot of chalcophile element concentrations in samples from Thompson Mine. From Liwanag (2001).

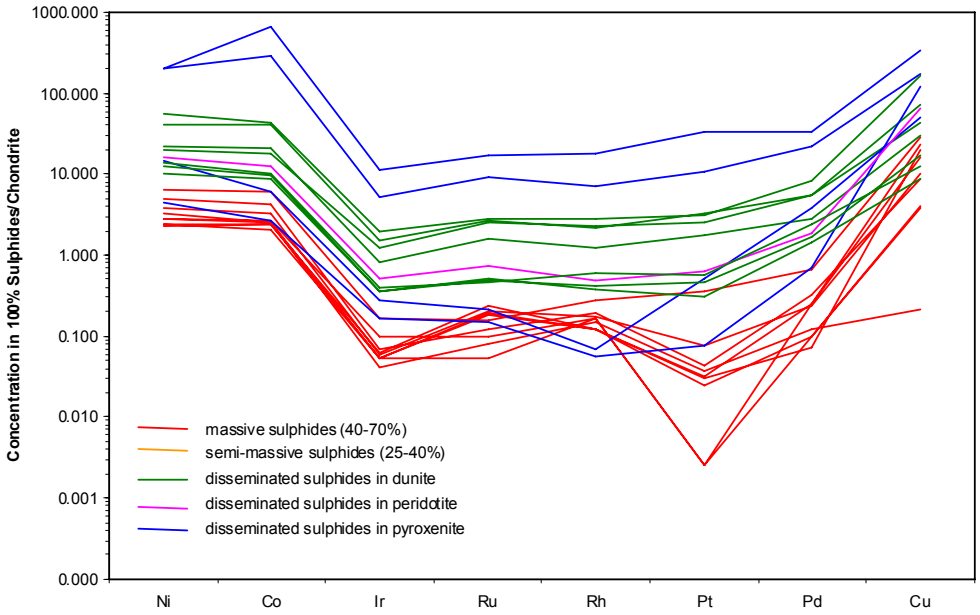

Figure 9.40 Chondrite-normalized plot of chalcophile element concentrations in samples from the Pipe deposit. From Liwanag (2001).

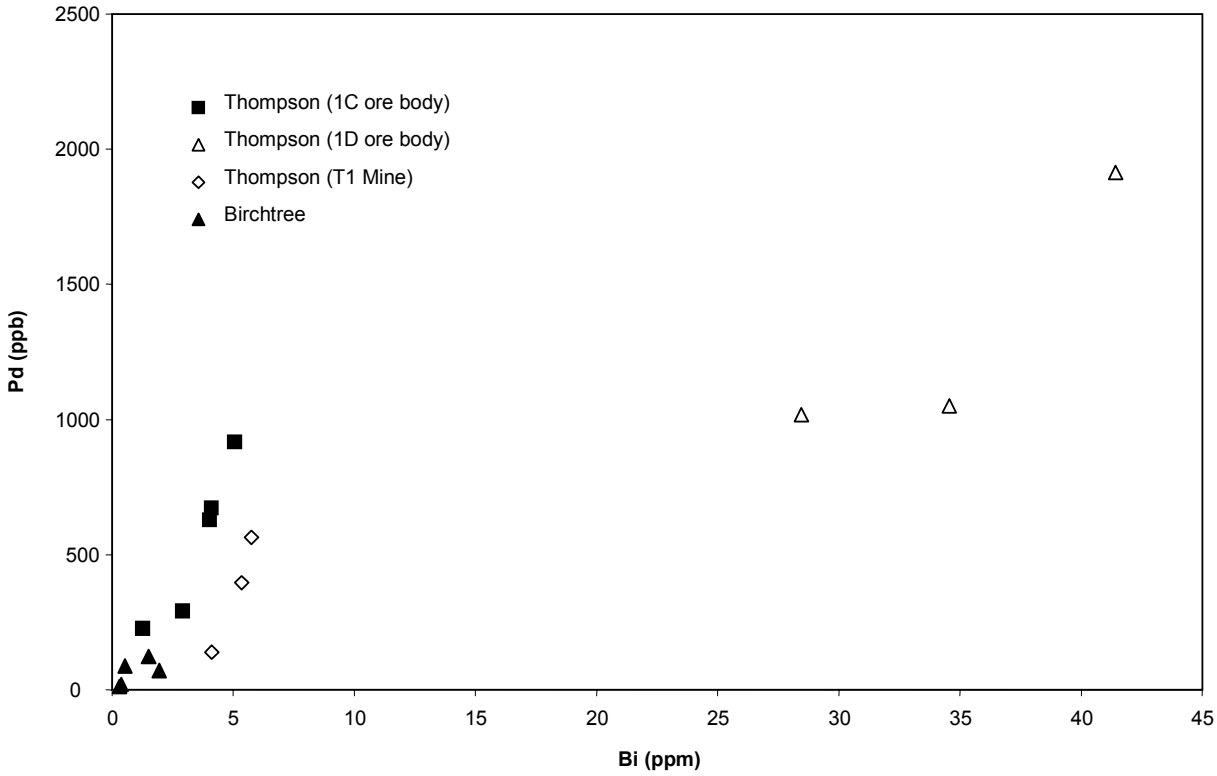

Figure 9.41 Pd and Bi concentrations in massive and semi-massive sulfide samples from the TNB. From Liwanag (2001).

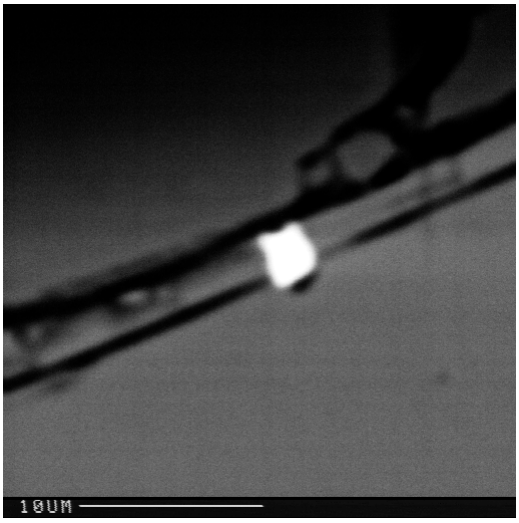

a

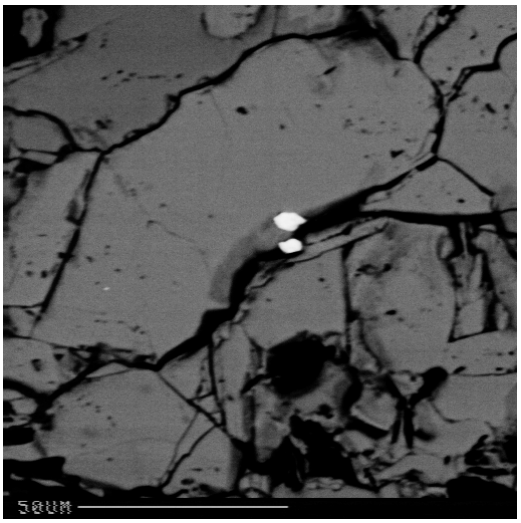

b

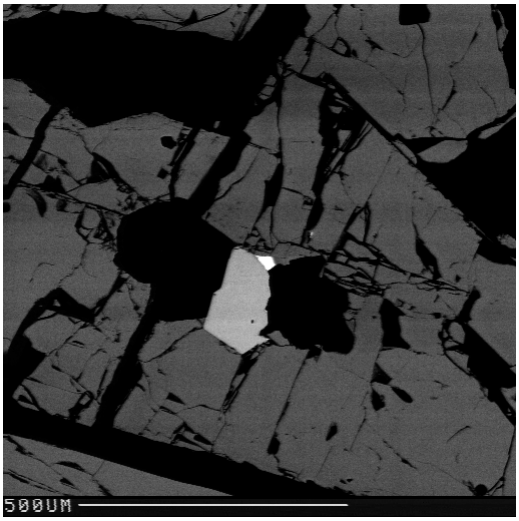

c

Figure 9.42 Bismuthotellurides in massive sulfides from the 1D ore body, Thompson mine. a) Pd-Bi-Te-bearing mineral (white) in pentlandite. b) Bi-Te-bearing grain (white) in pentlandite. c) Bi-Te-bearing grain (white) adjacent to gersdorffite (light grey), in pentlandite. From Liwanag (2001).

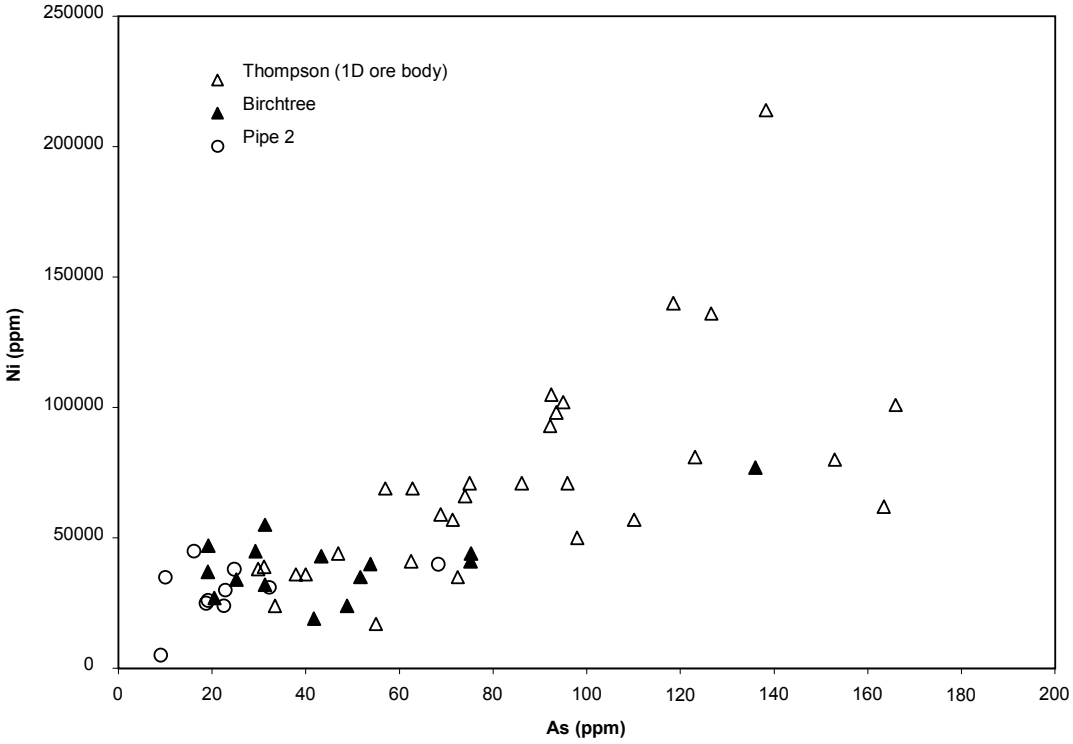

Figure 9.43 Ni and As concentrations in massive and semi-massive sulfides from the TNB. Sulfide classes represented: MS-UB, MS-SED, SMS-SED. From Liwanag (2001).

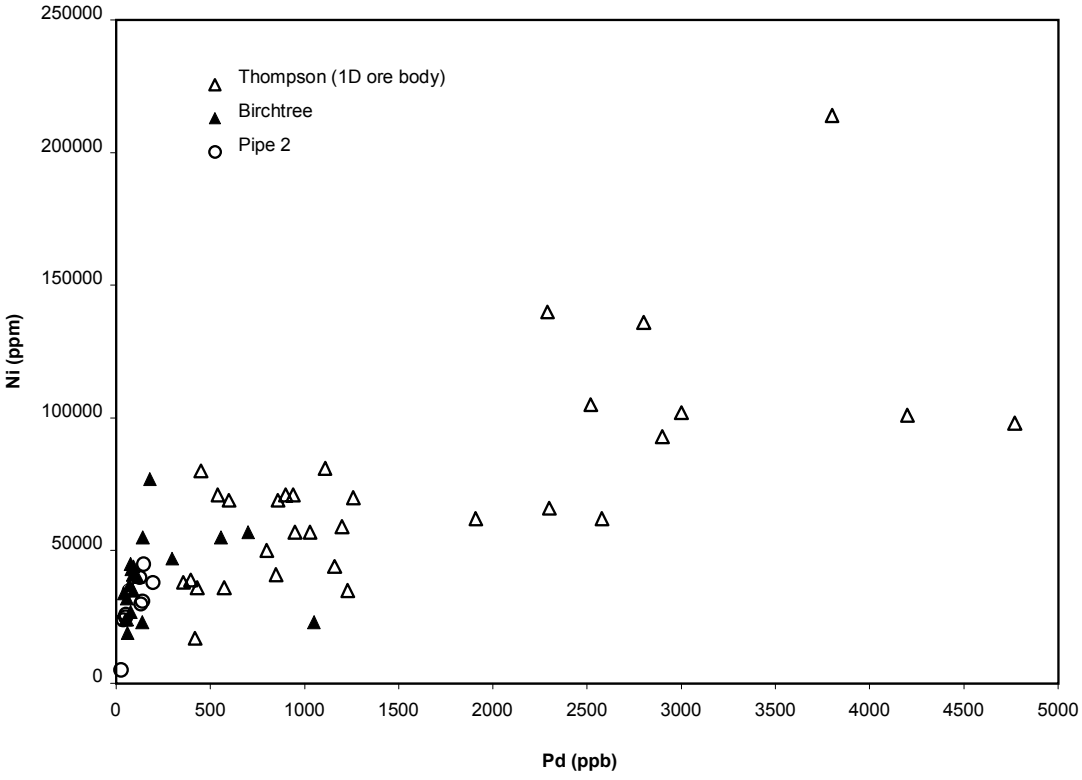

Figure 9.44 Ni and Pd concentrations in massive and semi-massive sulfides from the TNB. Sulfide classes represented: MS-UB, MS-SED, SMS-SED. From Liwanag (2001).

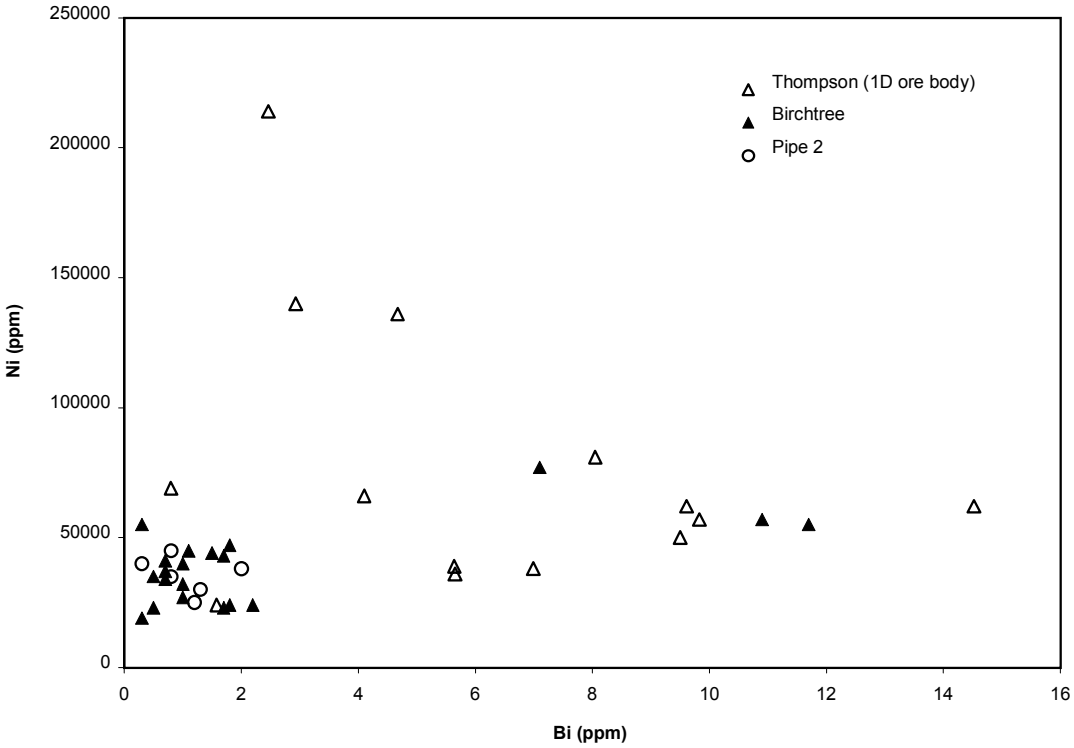

Figure 9.45 Ni and Bi concentration in massive and semi-massive sulfides from the TNB. Sulfide classes represented: MS-UB, MS-SED, SMS-SED. From Liwanag (2001).

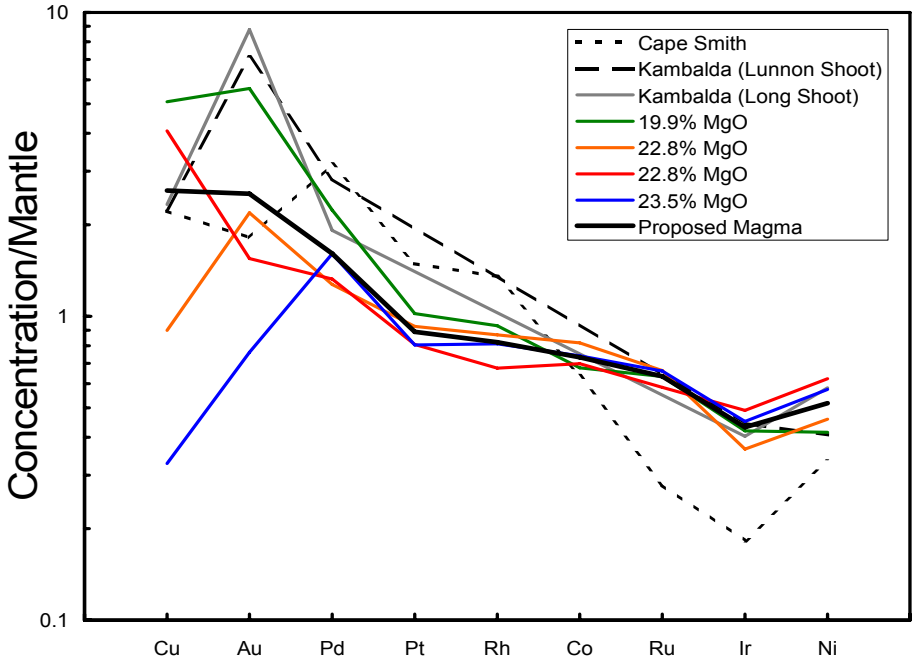

Figure 9.46 Chalcophile element compositions of parental magmas to TNB ultramafic bodies. Kambalda data from Keays (1982); Cape Smith data from Burnham & Lesher (unpubl., 1999). Mantle normalization values from McDonough & Sun (1995). Note that the reversals in Cu and Ni on this diagram are artefacts of those elements not being located in their proper locations with respect to compatibility (see discussion by Lesher and Keays, 2002).

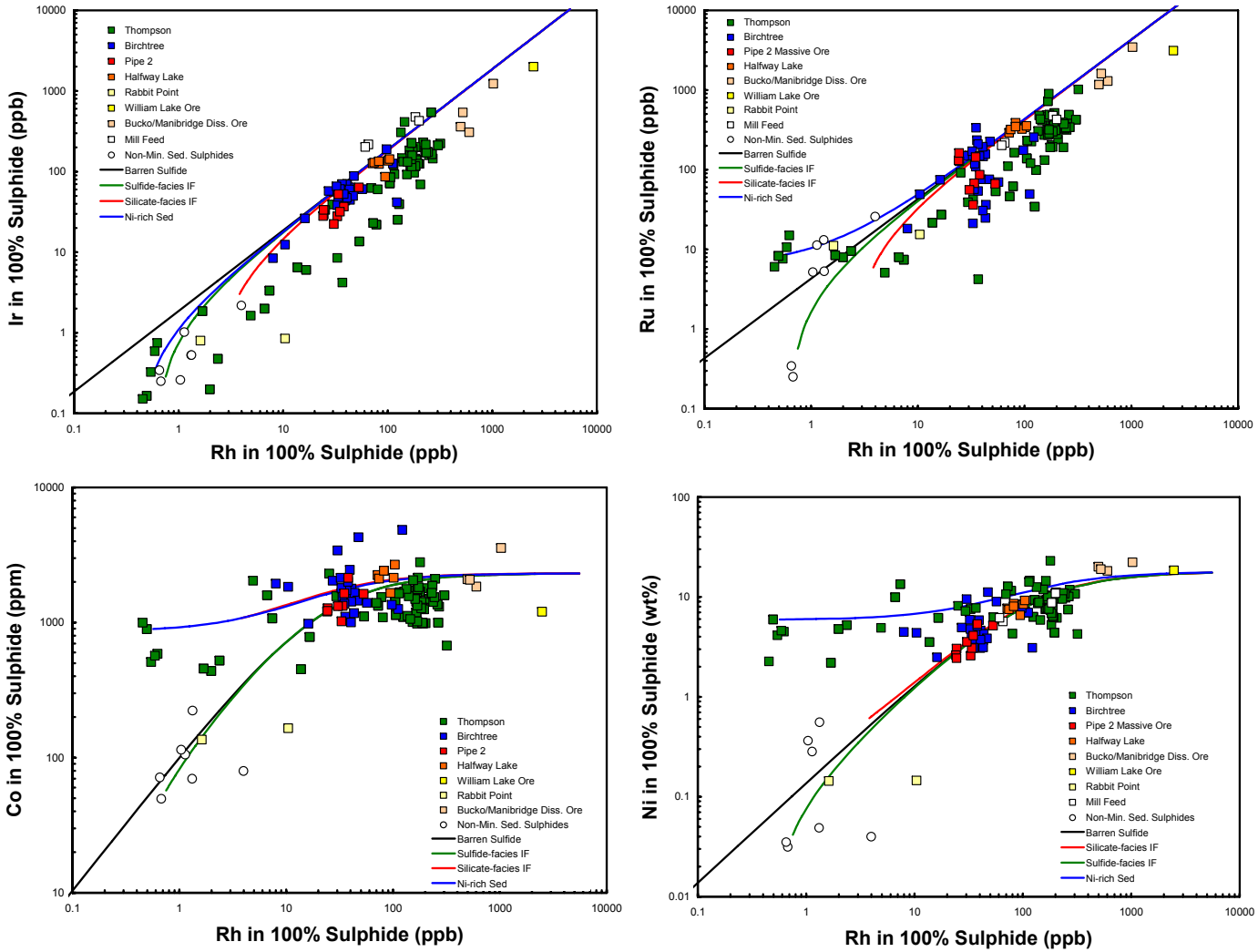

Figure 9.47 Compositions of magmatic sulfides produced for different R factors and metal contents in the external sulfide liquid. Only samples with > 4% S are plotted so as to minimize the relative contribution of metals from the silicate phases. Data from this study, CAMIRO Project 94E04, and an unpublished compilation by L. Hulbert. For values used in the modeling, see **Table 9.4.**

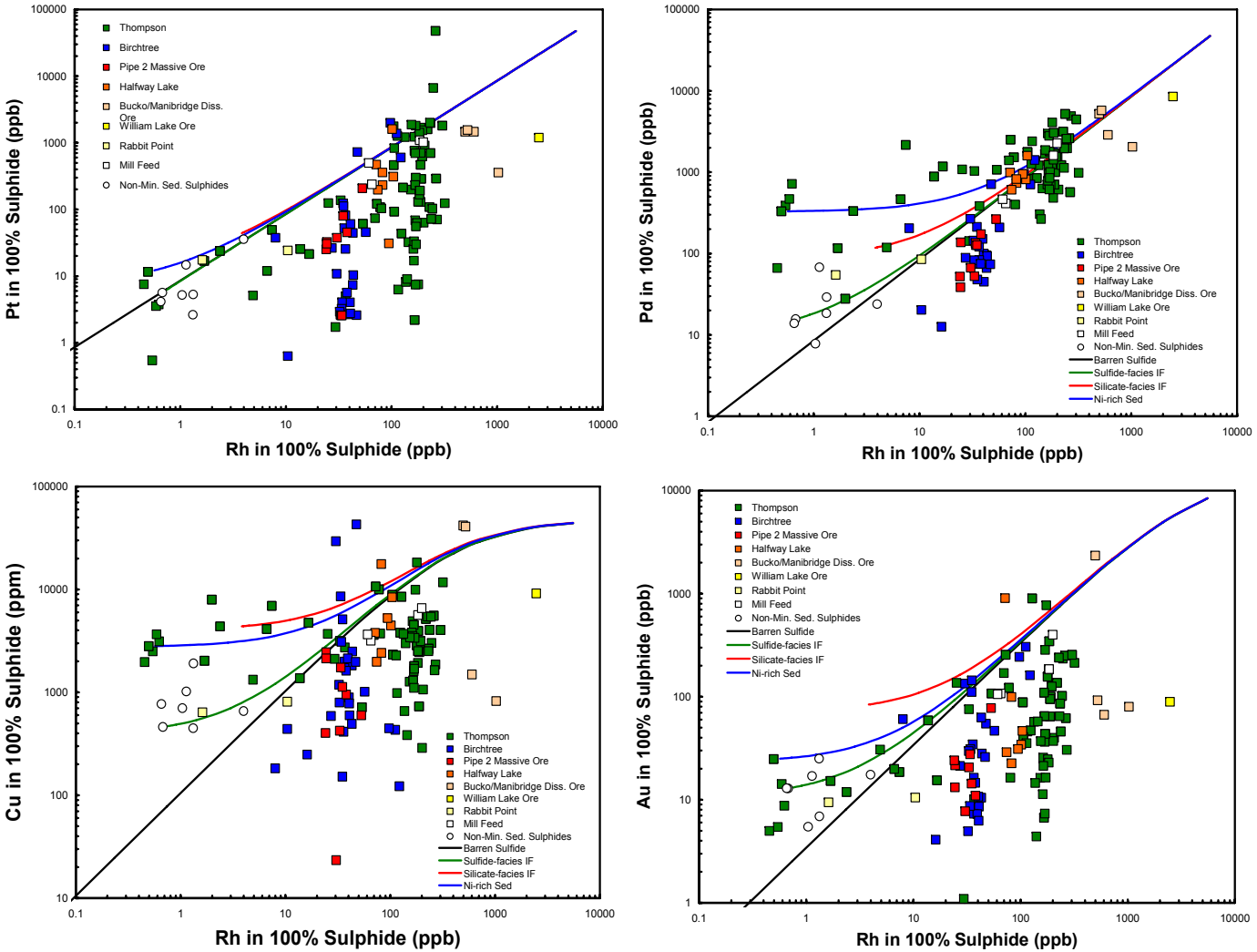

Figure 9.47 (cont.) Compositions of magmatic sulfides produced for different R factors and metal contents in the external sulfide liquid. Only samples with > 4% S are plotted so as to minimize the relative contribution of metals from the silicate phases. Data from this study, CAMIRO Project 94E04, and an unpublished compilation by L. Hulbert. For values used in the modeling, see **Table 9.4.**

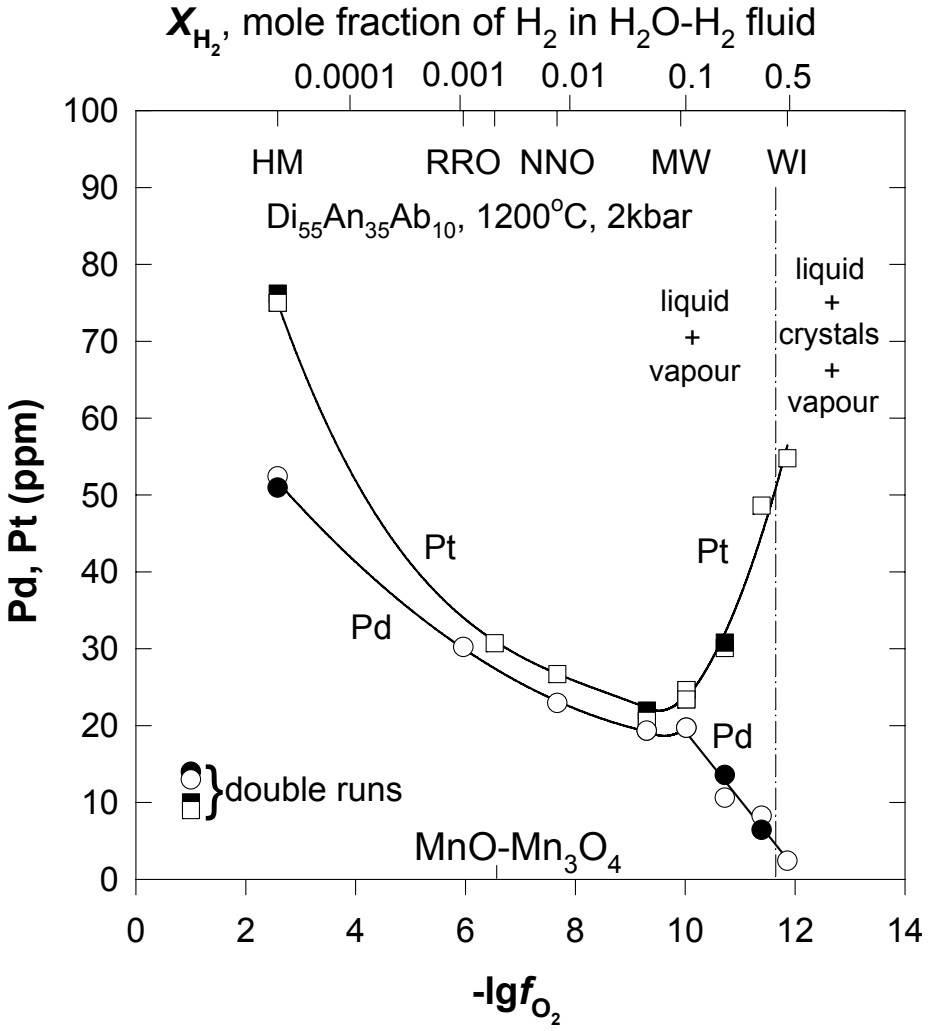

Figure 9.48 Solubility of Pd and Pt in the hydrous silicate melt *versus* oxygen fugacity (from Bezmen *et al.*, 1998).

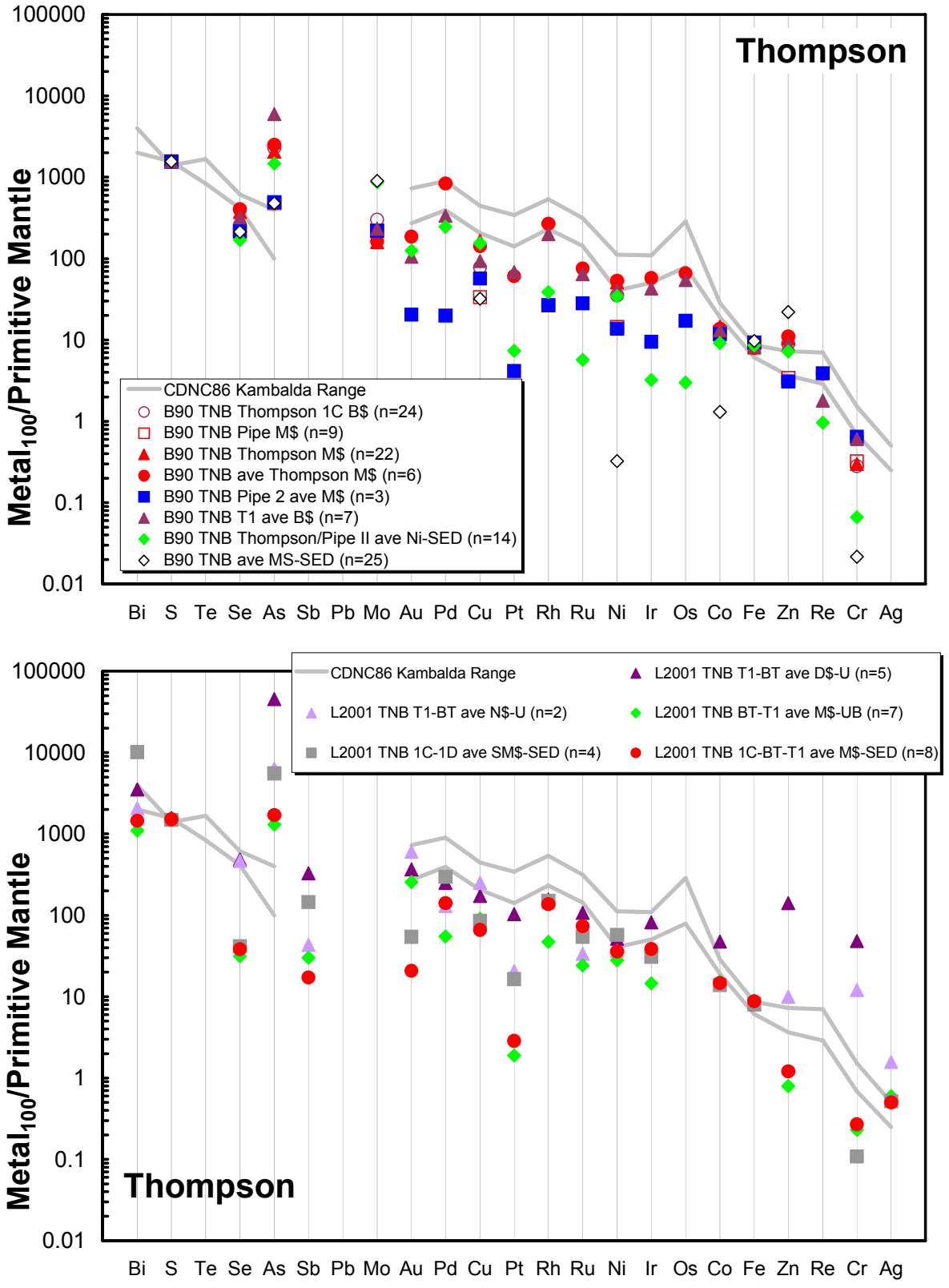

Figure 9.49 (a and b) Mantle-normalized chalcophile element patterns (data from Bleeker, 1990; Liwanag, 2001). Normalizing values from McDonough and Sun (1995).

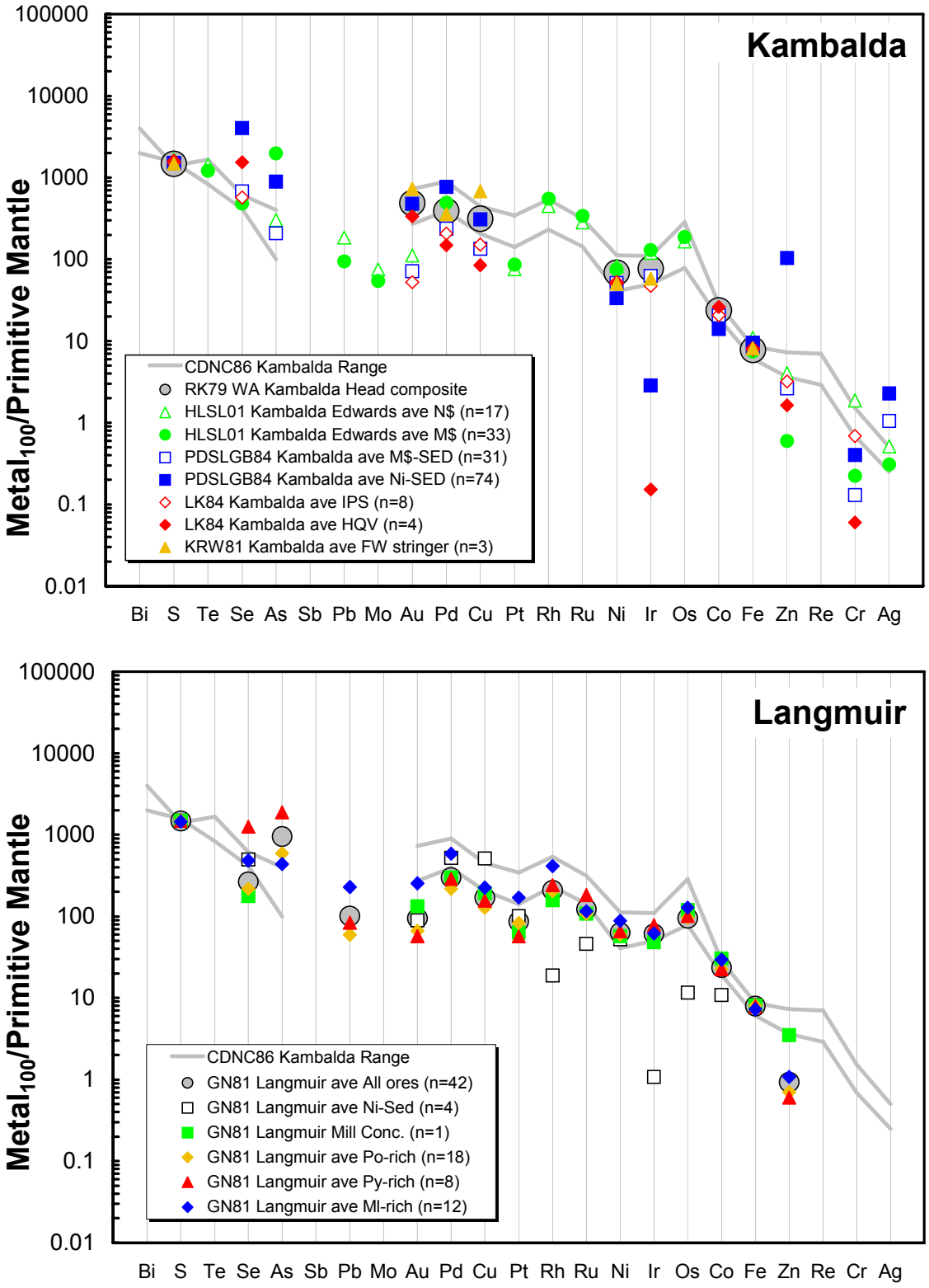

Figure 9.49 (c and d) Mantle-normalized chalcophile element patterns for Kambalda (data from Ross and Keays, 1979; Heath et al., 2001; Paterson et al., 1984; Lesher and Keays, 1984; Keays et al., 1981) and Langmuir (data from Green and Naldrett, 1981).

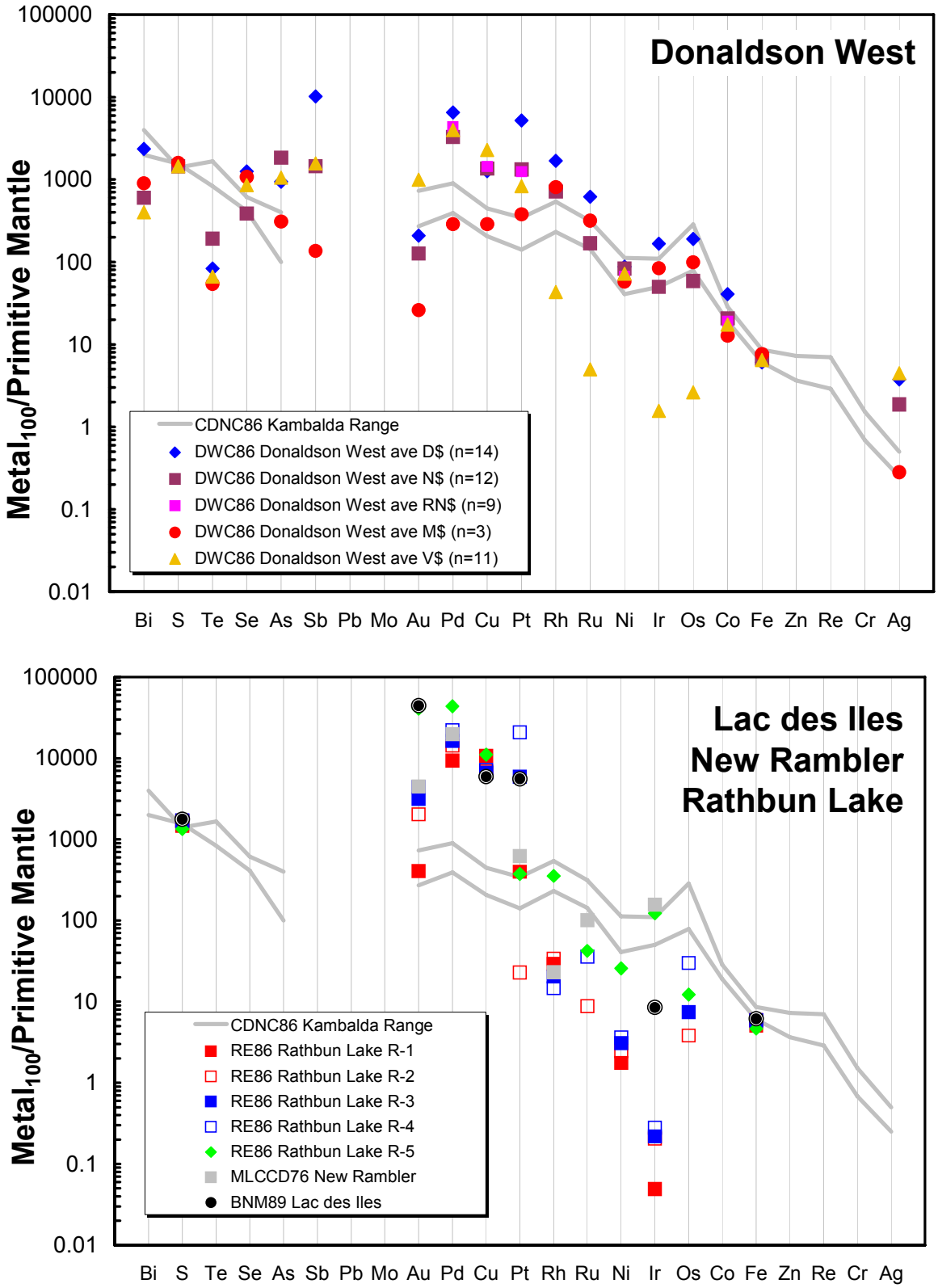

Figure 9.49 (e and f) Mantle-normalized chalcophile element patterns for Donaldson West (Dillon-Leitch et al., 1986), Lac des Iles (data from Brügmann et al., 1989), and New Rambler (data from Rowell and Edgar, 1986), Rathbun Lake (data from McCallum et al., 1976).

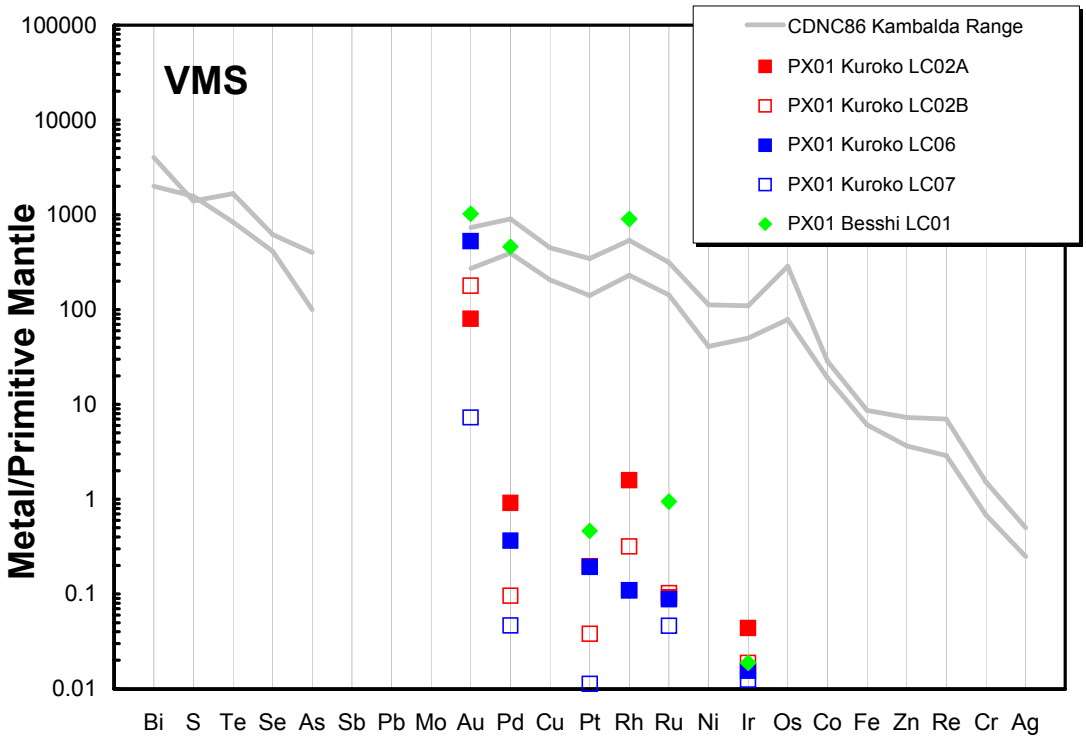

Figure 9.49 (g) Mantle-normalized chalcophile element patterns for Kuroko and Besshi VMS ores (data from Pan and Xie, 2001).

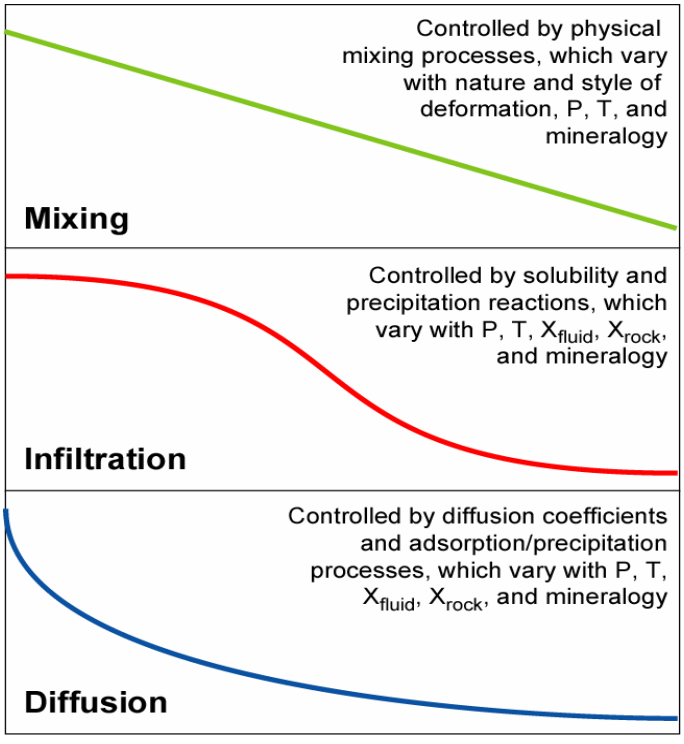

Figure 9.50 Schematic model showing theoretical variations in metal concentration profiles for physical mixing, fluid infiltration, and solid-state diffusion. Synchronous deformation will modify the profiles.

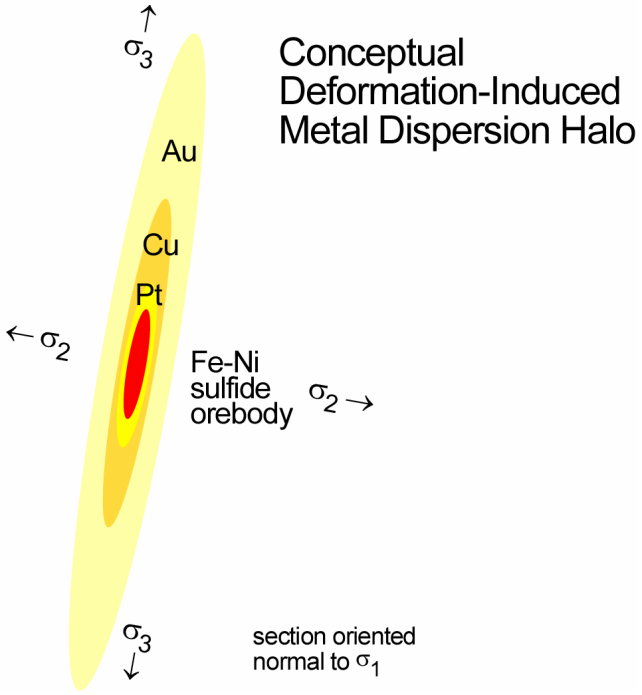

Figure 9.51 Schematic geochemical dispersion model for an ore deposit in the TNB that has been deformed transpressively, mobilizing Au > Cu > Pt >>> Pd ~ IPGE ~ Ni ~ Co ~ Cr.

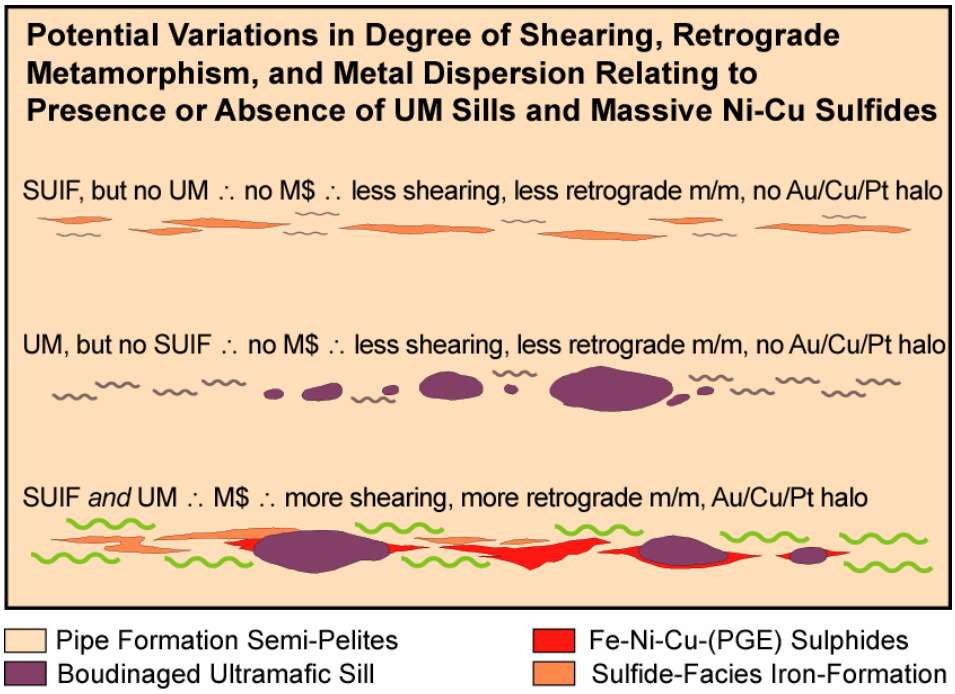

Figure 9.52 Schematic model showing variations in Au/Cu/Pt dispersion accompanying variations in deformation. With all else equal (e.g., original ore composition) less deformed systems will exhibit less dispersion and more deformed systems will exhibit more dispersion.